Article

A Single Human-Relevant Fast Food Meal Rapidly Reorganizes Metabolomic and Transcriptomic Signatures in a Gut Microbiota-Dependent Manner

Lucas J. Osborn [1,2,3,†], Danny Orabi [1,2,3,4,†], Maryam Goudzari [5], Naseer Sangwan [1,2], Rakhee Banerjee [1,2], Amanda L. Brown [1,2,3], Anagha Kadam [1,2], Anthony D. Gromovsky [1,2,3], Pranavi Linga [1,2], Gail A. M. Cresci [6], Tytus D. Mak [7], Belinda B. Willard [5], Jan Claesen [1,2,3,*], J. Mark Brown [1,2,3,*]

[1] Department of Cardiovascular and Metabolic Sciences, Lerner Research Institute of the Cleveland Clinic, Cleveland, OH 44195, USA

[2] Center for Microbiome and Human Health, Lerner Research Institute of the Cleveland Clinic, Cleveland, OH 44195, USA

[3] Department of Molecular Medicine, Cleveland Clinic Lerner College of Medicine of Case Western Reserve University, Cleveland, OH 44195, USA

[4] Department of General Surgery, Cleveland Clinic, Cleveland, OH 44195, USA

[5] Mass Spectrometry Core, Lerner Research Institute of the Cleveland Clinic, Cleveland, OH 44195, USA

[6] Department of Inflammation and Immunity, Lerner Research Institute of the Cleveland Clinic, Cleveland, OH 44195, USA

[7] Mass Spectrometry Data Center, National Institute of Standards and Technology, Gaithersburg, MD 20899, USA

† These authors contributed equally to this work.

* Correspondence: Jan Claesen, Email: claesej@ccf.org; Tel.: +1-216-636-3246; J. Mark Brown, Email: brownm5@ccf.org; Tel.: +1-216-444-8340.

ABSTRACT

Background: A major contributor to cardiometabolic disease is caloric excess, often a result of consuming low cost, high calorie fast food. Studies have demonstrated the pivotal role of gut microbes contributing to cardiovascular disease in a diet-dependent manner. Given the central contributions of diet and gut microbiota to cardiometabolic disease, we hypothesized that microbial metabolites originating after fast food consumption can elicit acute metabolic responses in the liver.

Methods: We gave conventionally raised mice or mice that had their microbiomes depleted with antibiotics a single oral gavage of a liquified fast food meal or liquified control rodent chow meal. After four hours, mice were sacrificed and we used untargeted metabolomics of portal and peripheral blood, 16S rRNA gene sequencing, targeted liver metabolomics, and host liver RNA sequencing to identify novel fast food-derived microbial metabolites and their acute effects on liver function.

Results: Several candidate microbial metabolites were enriched in portal blood upon fast food feeding, and were essentially absent in antibiotic-treated mice. Strikingly, at four hours post-gavage, fast food consumption

resulted in rapid reorganization of the gut microbial community and drastically altered hepatic gene expression. Importantly, diet-driven reshaping of the microbiome and liver transcriptome was dependent on an intact microbial community and not observed in antibiotic ablated animals.

Conclusions: Collectively, these data suggest a single fast food meal is sufficient to reshape the gut microbial community in mice, yielding a unique signature of food-derived microbial metabolites. Future studies are in progress to determine the contribution of select metabolites to cardiometabolic disease progression and the translational relevance of these animal studies.

KEYWORDS: microbiome; metabolomics; nutrition; circadian

ABBREVIATIONS

MetS, metabolic syndrome; TMA, trimethylamine; Fmo3, flavin-containing monooxygenase 3; TMAO, trimethylamine-*N*-oxide; DADA, divisive amplicon denoising algorithm pipeline; NMDS, non-metric multidimensional scaling; FDR, false discovery rate; ANOVA, analysis of variance; PERMANOVA, permutational multivariate analysis of variance; LCMS, liquid chromatography–mass spectrometry; QC, quality control; UHPLC, Ultra-High-Performance Liquid Chromatography; ESI, electrospray ionization; MS, mass spectrometry; LPA, lysophosphatidic acid; MS/MS, Tandem Mass Spectrometry; IQR, interquartile range; KEGG, Kyoto Encyclopedia of Genes and Genomes; HMDB, Human Metabolome Database; LIPID MAPS, Lipid Metabolites and Pathways Strategy; PCA, principal component analysis; SRA, Sequence Read Archive**;** RT-qPCR, real time quantitative polymerase chain reaction; *m*/z_RT, mass-to-charge ratio_retention time

INTRODUCTION

Metabolic syndrome (MetS) is a pervasive disorder impacting roughly one in three adults in the United States [1]. Individuals with MetS have an increased propensity to develop cardiovascular-related diseases and have higher incidence of all-cause mortality [2,3]. Although many factors may contribute to the development and progression of MetS, a surplus of dietary caloric intake represents a common and preventable disease risk factor. The increasing availability of low-cost, high-calorie, convenient food undoubtedly contributes to what has been described as the American obesity epidemic [2]. Recent controlled studies have revealed that a fixed dietary input amongst a group of individuals does not necessarily equate to a fixed output [4–7]. The variability associated with these findings is largely attributed to inter-individual variation in gut microbial composition. An excellent example of this concept is the consumption of foods rich in choline, phosphatidylcholine, and carnitine. Most omnivorous humans contain gut microbes with trimethylamine (TMA) lyase enzymes that convert these dietary substrates into TMA. TMA is then

converted by host flavin-containing monooxygenase 3 (Fmo3) into trimethylamine-*N*-oxide (TMAO), a pro-atherogenic, pro-thrombotic molecule [8–10]. Strikingly, vegans almost universally lack gut microbes capable of converting carnitine into TMA and thus do not produce TMAO after consuming red meat [4].

Traditionally, rodent models of MetS are achieved through ad libitum feeding of a lard based diet containing 60% of calories from fat. While effective in promoting obesity, hyperglycemia, and insulin resistance, these diets are not representative of a human diet. In order to better understand the interface between diet, the gut microbiome, microbial metabolites, and MetS, we herein propose to explore the use of a human-relevant diet.

In this study, we aimed to identify microbe-derived metabolites stemming from consumption of a human-relevant fast food meal. In pursuit of this aim, we fed a single meal equivalent of either rodent chow or fast food to conventionally raised mice (with an intact gut microbiome) and mice that had their microbiota ablated with antibiotics. We discovered a rapid reorganization of the gut microbial community structure that was independent of microbes that might have been associated with the meals. Moreover, we identified unique gut microbe-derived metabolites that were enriched in the portal blood of mice receiving an oral gavage of fast food compared to those receiving chow. Distinct transcriptional profiles were identified in the liver with notable diet and gut microbial dependencies. Taken together, these data represent a multi-omics approach to identify novel gut microbe-derived transcriptional and metabolic signatures that arise postprandially after consumption of a fast food meal. Future studies are in progress to determine which of these metabolites are causally linked to MetS.

MATERIALS AND METHODS

Animal Studies

6-week old male C57BL6/J mice were purchased from Jackson Laboratories (Bar Harbor, ME, USA) and randomly assigned to control drinking water or drinking water supplemented with vancomycin (0.5 g/L), neomycin (1 g/L), ampicillin (1 g/L), and metronidazole (1 g/L) and maintained on a defined rodent chow (TD.130104) for two weeks (*n* = 6–7 per group). Next, mice were fasted overnight and at the beginning of the light cycle were given a single oral gavage (0.2 mL) of either liquified chemically defined chow (TD.130104) from Harlan Laboratories (Madison, WI) or liquified fast food (procured from local fast food restaurants) and sacrificed exactly 4 h later. The 4 h postprandial time point was chosen based on previous studies showing the production of the gut microbe-associated co-metabolites trimethylamine (TMA) and trimethylamine *N*-oxide (TMAO) peak ~2–4 h after a high fat meal [11,12]. Our goal was to choose a relevant time point where gut microbes would be actively producing metabolites from the dietary substrates provided. To accurately

model a human-relevant fast food meal, food items were purchased from three of the top five grossing fast food chains in the USA (McDonald's, Taco Bell, and Burger King). All food was ordered locally in Cleveland, Ohio with instructions to the servers to exclude any vegetable products (i.e., no lettuce, tomato, onion, etc.). The actual items used to make the liquified fast food meal are shown in Figure 1, and included the following popular menu items: (1) McDonald's double quarter pounder with cheese, (2) McDonald's chicken tenders, (3) McDonald's French fries, (4) Burger King Whopper with cheese, (5) Burger King original chicken sandwich, (6) Burger King cheesy tots, (7) Burger King French fries, (8) Taco Bell beef crunchy taco, (9) Taco Bell chicken quesadilla, and (10) Taco Bell 5 layer burrito. To mimic what the human intestine sees after a fast food meal, the items above were minced into a solvent of Coca Cola and a McDonald's chocolate milkshake using an industrial blender. The resulting fast food slurry or a control slurry of rodent chow (TD.130104) in water solvent was administered via oral gavage, and exactly 4 h postprandially mice were terminally anesthetized with ketamine/xylazine (100–160 mg/kg ketamine -20–32 mg/kg xylazine), and a midline laparotomy was performed. A small volume (~50–100 μL) of blood was collected directly from the portal vein (i.e., blood draining from the gut where microbe-derived metabolites are enriched), and the remaining peripheral blood was collected via cardiac puncture. Following blood collection, a whole body perfusion was conducted by puncturing the inferior vena cava and slowly delivering 10 mL of saline into the heart to remove blood from tissues. Tissues were collected and immediately snap frozen in liquid nitrogen for subsequent biochemical analysis or fixed for morphological analysis. All animal procedures were approved on September 9, 2016 under protocol 2016-1631 by the Institutional Animal Care and Use Committee of the Cleveland Clinic.
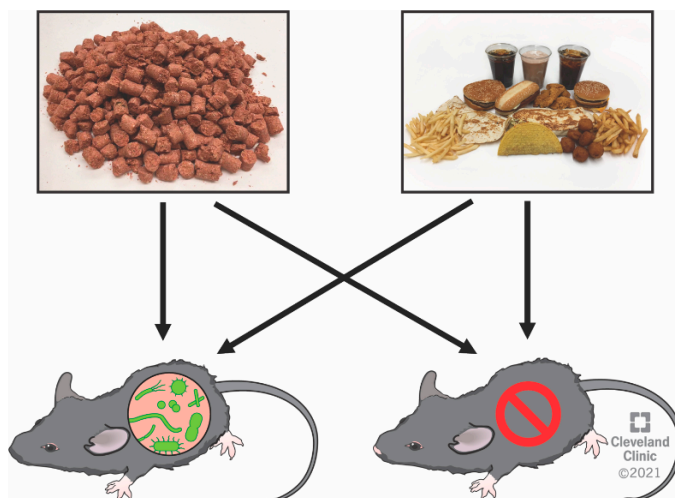

Figure 1. Experimental Design to Identify Fast Food-Derived Gut Microbial Metabolites. 6-week old male C57BL6/J mice were randomly assigned to normal drinking water or drinking water supplemented with vancomycin (0.5 g/L), neomycin (1 g/L), ampicillin (1 g/L), and metronidazole (1 g/L) for two weeks. Next, mice were given a single oral gavage of either chow slurry or fast food slurry and sacrificed 4 h later for phenotypic characterization.

Cecal and Food Microbiome Analyses

DNA was extracted from mouse cecal contents and food samples using the QIAGEN PowerSoil Pro kit using the manufacturer's protocol. 16S rRNA amplicon sequencing was done for the V1-V2 region using Illumina MiSeq at 2 × 250 cycles from mouse cecal contents and food samples. Raw 16S amplicon sequences and metadata were demultiplexed using the *split_libraries_fastq.py* script implemented in *QIIME1.9.1* [13]. The demultiplexed fastq file was split into sample specific fastq files using the *split_sequence_file_on_sample_ids.py* script from *QIIME1.9.1* [13]. Individual fastq files without non-biological nucleotides were processed using the Divisive Amplicon Denoising Algorithm (DADA) pipeline [14]. The output of the DADA2 pipeline (feature table of amplicon sequence variants) was processed for alpha and beta diversity analysis using the *phyloseq* [15] and *microbiomeSeq* packages (http://www.github.com/umerijaz/microbiomeSeq) in R. Alpha diversity estimates were measured within group categories using the *estimate_richness* function of the *phyloseq* package [15]. Non-metric multidimensional scaling (NMDS) was performed using the Bray-Curtis dissimilarity matrix [16] between groups and visualized by using the *ggplot2* package [17]. We assessed the statistical significance ($p < 0.05$) throughout, and whenever necessary we adjusted *p*-values for multiple comparisons according to the Benjamini-Hochberg method to control false discovery rate (FDR) [18] while performing multiple testing on taxa abundance according to sample categories. We performed an analysis of variance (ANOVA) among sample categories while measuring the alpha diversity measures using the *plot_anova_diversity* function in the *microbiomeSeq* package. Permutational multivariate analysis of variance (PERMANOVA) with 999 permutations was performed on all principal coordinates obtained during principal coordinates analysis with the *ordination* function of the *microbiomeSeq* package. Linear regression (parametric) and Wilcoxon (non-parametric) tests were performed on amplicon sequence variant abundances against meta-data variable levels using their base functions in R [19].

Plasma Untargeted Metabolomics

Portal blood was collected from the portal vein and peripheral blood via cardiac puncture at time of necropsy. Blood was centrifuged at 5000 × *g* for 5 min and the plasma fraction was processed via liquid chromatography-mass spectrometry (LCMS). Plasma samples were prepared by diluting each sample 1:20 in chilled methanol containing isotopically labeled internal standards. The samples were then vortexed and centrifuged at 14,000 × *g* for 20 min to precipitate out the protein pellet. The supernatants were recovered for LCMS analysis. One-microliter aliquots taken from each sample were pooled and technical replicates of this quality control (QC) standard were analyzed every 10 injections. 5 µL of each sample was injected onto a 10 cm C18 column (Thermo Fisher, CA, USA) coupled to a

Vanquish Ultra-High-Performance Liquid Chromatography (UHPLC+ focused) system running at 0.35 mL/min using water and 0.1% formic acid as solvent A and acetonitrile and 0.1% formic acid as solvent B. A 15-min gradient of [time(minutes)]:[%solvent B] of [0.2,1,8,10,12,14]:[5,15,95,95,5,5] was used. The Orbitrap Q-Exactive HF was operated in positive and negative electrospray ionization (ESI) modes covering a mass range of 56-850 Da using full mass spectrometry (MS) scans at 120,000 resolution. Data-dependent MS^2 spectra from the pooled QC sample were acquired on the top 10 most abundant ions at a resolution of 30,000 with dynamic exclusion of 40.0 s and the apex trigger set at 2.0 to 4.0 s. The resolution of the MS^2 scans were taken at a stepped normalized collision energy of 20.0, 30.0, and 45.0. Lockmass was applied in both ESI modes and the full MS data were acquired in profile mode. Validation of 18:0 lysophosphatidic acid (LPA) was performed via tandem mass spectrometry (MS/MS) against a commercial standard(Avanti Polar Lipid, Inc. product no. 857128P). Additional reference spectral libraries, including Metlin (https://metlin.scripps.edu) and mzCloud (https://www.mzcloud.org) were searched for additional information on collision energy and structural elucidations. XCMS (xcmsonline.scripps.edu) was used to deconvolute the untargeted metabolomics data using 5 ppm consecutive scan error, 8 to 45 s as minimum and maximum peak width, and a signal-to-noise threshold of 10.

The resulting peak tables (Supplementary File S1A,B) were further analyzed using MetaboLyzer as previously described to perform single two-group analysis [20]. Briefly, the data were natural log transformed and ions present in at least 70% of the samples in all study groups at non-zero abundances (complete-presence ions) were analyzed via traditional statistical methods. Outliers were removed via 1.5 interquartile range (IQR) filtering, and the non-parametric Mann-Whitney U test ($p < 0.05$) was utilized to determine statistical significance. Ions that met the 70% presence threshold in only one group (partial-presence ions) were analyzed categorically via Fisher's exact test. All p-values were corrected via the adjusted Benjamini-Hochberg correction procedure [18,21], with an FDR q-value threshold of 0.1 (10%) to delineate significance. MetaboLyzer was also used for putative identification of ions at maximum m/z tolerance of 7 ppm using the Kyoto Encyclopedia of Genes and Genomes (KEGG) [22], Human Metabolome Database (HMDB) [23], Lipid Metabolites and Pathways Strategy (LIPID MAPS) [24], and BioCyc Database Collection [25] (Supplementary File S1C,D). Metabolyzer offered a deep understanding of single two-group analyses, generating volcano plots, principal component analysis (PCA) score plots, and metabolic pathway enrichment plots.

In addition, a novel Python programming language (v3.7.0) script was used to perform several two-group analyses simultaneously to identify ions that satisfied a complete set of user-specified comparison criteria (Supplementary File S3). Ions absent in greater than 50% of all samples

were excluded from analysis. Zeros were converted to half the lower limit of detection, defined by the lowest intensity value of all samples for that ion. Values were natural log converted. Outlier values were removed via 1.5 IQR filtering and excluded from analysis. For each user-specified two-group comparison, the Mann-Whitney U test was used to generate p-values, then an adjusted Benjamini-Hochberg correction procedure was performed to determine q-values [18,21]. An FDR q-value threshold of 0.1 (10%) was used to delineate significance. Desired comparison criteria were specified by the user (e.g., significant increase from group 1 to group 2, significant decrease from group 2 to group 3, etc.), and ions meeting all comparison criteria i.e., hits were displayed with their relevant information including putative ID if available. To rank their fitness of the comparison criteria listed, hits were scored based on user-specified weights for fold-change differences between groups of each comparison, and were displayed in order of fitness. Values were reconverted to exponential form, and bar graphs were made with GraphPad Prism (v9.0.0).

Liver Targeted Metabolomics

The AbsoluteIDQ® p400 HR kit from Biocrates Life Sciences AG was used to obtain targeted quantitative metabolomics data. Liver tissue was collected at time of necropsy following transcardial saline perfusion. The liver tissue samples were prepared according to manufacturer protocol. Briefly, at least 30 mg of each tissue sample was cut and weighed, and kept frozen throughout this protocol. The tissue samples were homogenized and centrifuged at 10,000 × g for 5 min. The supernatant was then collected, 10 µL of which per sample was loaded onto a 96-well plate containing stable isotope-labeled standards, and processed according to manufacturer protocol. The LCMS analysis was done using specific parameters (both Tune and LCMS methods) per kit manufacturer's recommendations. The assay was performed on a Q-Exactive HF (operated only in positive ESI mode) coupled with a Vanquish UHPLC+ focused liquid chromatography as detailed per assay instructions. The manufacturer-provided software, Met*IDQ* (Biocrates, Life Science AG), was used to provide the resultant peak table (Supplementary File S2). Python programming language (v3.7.0) was used to analyze the data (Supplementary File S4). Molecules absent in greater than 50% of samples were excluded from analysis. Outlier values were removed via 1.5 IQR filtering and excluded from analysis. Comparisons were performed using the Mann-Whitney U test to generate p-values, then an adjusted Benjamini-Hochberg correction procedure was performed to determine q-values [18,21]. An FDR q-value threshold of 0.15 (15%) was used to delineate significance. Z-scores were calculated for heatmap generation. Bar graphs and heatmaps were made with GraphPad Prism (v9.0.0).

Hepatic RNA Sequencing and Analysis

RNA was isolated via the RNeasy Plus Mini Kit (Qiagen, Hong Kong) from mouse liver following the manufacturer's protocol. RNA samples were checked for quality and quantity using the Bioanalyzer (Agilent,

Santa Clara, CA, USA). RNA-Seq libraries were generated using the Illumina mRNA TruSeq RNA library kit following Ribo-Zero depletion and sequenced using an Illumina HiSeq 4000 (all according to the manufacturer's instructions). RNA sequencing was performed by the University of Chicago Genomics Facility. Single 50 bp reads were controlled for quality with *FastQC* (https://www.bioinformatics.babraham.ac.uk/projects/fastqc/) before trimming Illumina adapters from the 3' ends using *cutadapt* [26]. *STAR* was used to align trimmed reads to the *Mus musculus* genome (NCBI GRCm38.93) [27]. Read counts for each gene were calculated using *HTseq* [28] and loaded into R (http://www.R-project.org/) (R Development Core Team, 2015) where *DESeq2* [29] (v.1.28.1, https://bioconductor.org/packages/release/bioc/html/DESeq2.html) was used to perform differential expression analysis on genes with at least 1 count per sample with alpha set to 0.05. *P*-values were adjusted using the Benjamini-Hochberg correction procedure [18] and genes with $p < 0.05$ were considered statistically significant. Heatmaps were generated of the top 50 differentially expressed transcripts using *pheatmap* [30] and *RColorBrewer* [31]. NMDS analysis was performed using the *plotMDS* function of *edgeR* [32] using the top 500 differentially expressed genes as sorted by log2 fold change. Pathway analysis on the top 150 differentially expressed genes was performed using *Metascape* [33]. The data discussed in this publication have been deposited in NCBI's Gene Expression Omnibus [34] and are accessible through GEO Series accession number GSE165756.

Real Time Quantitative PCR Analysis of Gene Expression

RNA was isolated via the RNeasy Plus Mini Kit (Qiagen, Hong Kong) from mouse liver following the manufacturer's protocol. Real time quantitative polymerase chain reaction (RT-qPCR) analyses were conducted as previously described [35–37]. *Gapdh* was used as a housekeeping gene for all RT-qPCR analyses and mRNA expression levels were calculated based on the ΔΔ-CT method. qPCR was conducted using the Applied Biosystems 7500 Real-Time PCR System. Primers used for RT-qPCR are available on request.

Total Hepatic Triglyceride, Cholesterol, and Phosphatidylcholine Analyses

The extraction of liver lipids and quantification of total hepatic triglyceride, free cholesterol, and phosphatidylcholine was conducted using enzymatic assays as described previously [38–40].

Oxygen Bomb Calorimetry

Samples of the chow and fast food slurries were placed into 10 mL falcon tubes and dried at 60 °C for 48 h. After 48 h, dried samples were weighed to 30–55 mg per sample. This weight (in grams) was recorded in the system software before the sample was combusted. Samples were placed in an 1109A Semimicro Oxygen Bomb containing a 10 cm fuse wire or 23 "units"

and filled with 35–40 psi oxygen. The samples were then combusted in a Parr Instruments 6725 semimicro calorimeter containing 450 grams of water. After combustion, the amount of fuse wire remaining was subtracted from 23 "units". This value was input into the system and the heat of combustion was generated. Heat of combustion was generated in cal/g.

Statistical Analysis

16S rRNA Sequencing: Statistical analysis of Shannon alpha diversity estimates was performed via ANOVA. PERMANOVA was used to analyze NMDS plots based on the Bray-Curtis index between the chow and fast food cecal contents as well as the microbial composition of the food itself. Statistical analysis of pairwise differential abundance was performed with White's non-parametric t-test. n = 6–7 per group.

Untargeted Plasma Metabolomics: The data were natural log transformed and ions present in at least 70% of the samples in all study groups at non-zero abundances (complete-presence ions) were analyzed via traditional statistical methods. Outliers were removed via 1.5 interquartile range (IQR) filtering, and the non-parametric Mann-Whitney U test ($p < 0.05$) was utilized to determine statistical significance. Ions that met the 70% presence threshold in only one group (partial-presence ions) were analyzed categorically via Fisher's exact test. All p-values were corrected via the adjusted Benjamini-Hochberg correction procedure [18,21], with an FDR q-value threshold of 0.1 (10%) to delineate significance. Additionally, simultaneous two-group analysis was performed to identify ions that satisfied a complete set of user-specified comparison criteria (Supplementary File S3). Ions absent in greater than 50% of all samples were excluded from analysis. Zeros were converted to half the lower limit of detection, defined by the lowest intensity value of all samples for that ion. Values were natural log converted. Outlier values were removed via 1.5 IQR filtering and excluded from analysis. For each user-specified two-group comparison, the Mann-Whitney U test was used to generate p-values, then an adjusted Benjamini-Hochberg correction procedure was performed to determine q-values [18,21]. An FDR q-value threshold of 0.1 (10%) was used to delineate significance. To rank the fitness of comparisons, hits were scored based on user-specified weights for fold-change differences between groups. Values were reconverted to exponential form. n = 4–7 per group.

Targeted Hepatic Metabolomics: Molecules absent in greater than 50% of samples were excluded from analysis. Outlier values were removed via 1.5 IQR filtering and excluded from analysis. Comparisons were performed using the Mann-Whitney U test to generate p-values, then an adjusted Benjamini-Hochberg correction procedure was performed to determine q-values [18,21] (Supplementary File S4). An FDR q-value threshold of 0.15 (15%) was used to delineate significance. Z-scores were calculated for heatmap generation. n = 6–7 per group.

RNA-Sequencing Analysis: Statistical analysis on differentially expressed genes was performed on genes with at least 1 count per sample with alpha set to 0.05. *P*-values were adjusted using the Benjamini-Hochberg correction procedure [18] and genes with $p < 0.05$ were considered statistically significant. n = 4 per group.

Quantitative-Real Time PCR: Statistical analysis of qPCR data was performed using a two-way ANOVA with Tukey's multiple comparison test. n = 6–7 per group.

Hepatic Lipid Analysis: Statistical analysis was performed using two-way ANOVA with Tukey's multiple comparisons test and significance is displayed for differences within each meal-type between gut microbiota groups (control vs antibiotic ablated) and within gut microbiota groups, between meal type. n = 6–7 per group.

Bomb Calorimetry: Statistical analysis was performed using two-way ANOVA with Tukey's multiple comparisons test and significance is displayed for differences within type of sample preparation. n = 3 per group.

RESULTS

A Single Fast Food Meal Promotes Rapid Remodeling of the Gut Microbiome

It is well known that dietary practices can have profound effects on gut microbiome communities in rodents and humans [41–43]. However, most studies focus on microbiome alterations after days or weeks of dietary manipulation. Here we set out to understand the acute postprandial effects of a human-relevant fast food meal on gut microbiome community structure in C57BL/6J mice. Exactly four hours after receiving a single meal equivalent of either fast food or rodent chow (Figure 1, Supplementary Figure S1, Supplementary Tables S1 and S2), cecal contents were harvested and profiled via 16S rRNA sequencing (Figure 2). In addition to the cecal contents, the rodent chow and human-relevant fast food meal slurries themselves were also profiled via 16S rRNA sequencing to understand the potential contribution of food-associated bacteria. Alpha diversity within each meal type was compared between control and antibiotic-treated groups (Figure 2A). Strikingly, just four hours after the oral gavage, distinct diet- and antibiotic-dependent clustering was observed (Figure 2B). Importantly, these rapid shifts in microbial community are independent of the 16S rRNA signals contained within the food slurries themselves (Figure 2B,C). Moreover, antibiotic treatment led to a striking reduction in the *Bacteroides* genus in fast food-gavaged mice (Figure 2C). Not surprisingly, the fast food slurry itself has a relatively low diversity microbiome associated with it, which is largely comprised of the food-associated commensal genera *Streptococcus, Lactococcus*, and *Lactobacillus* (Figure 2C) [44,45].
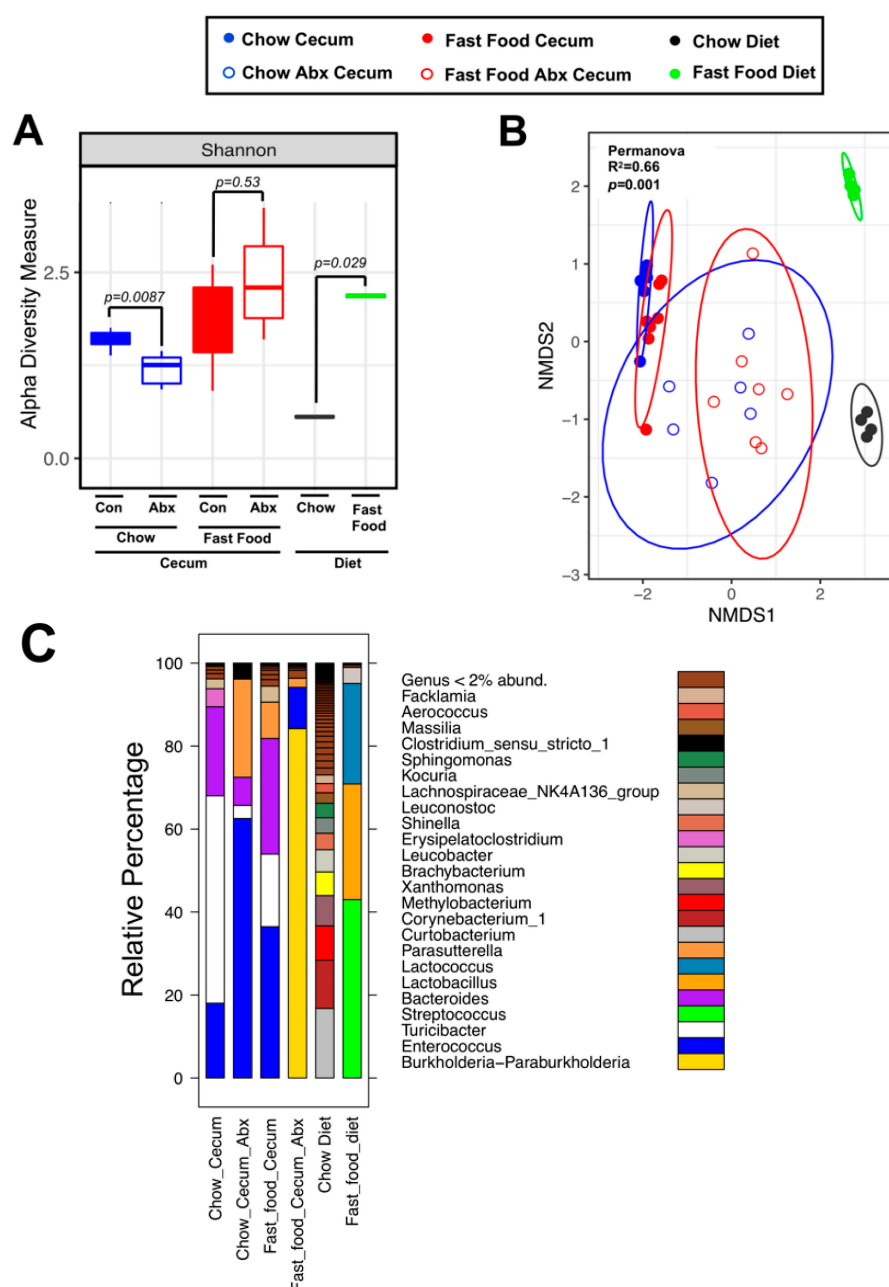
Figure 2. A Single Fast Food Meal Promotes Rapid Remodeling of the Gut Microbiome. 6-week old male C57BL6/J mice were randomly assigned to control drinking water or drinking water supplemented with broad spectrum antibiotics for two weeks. Following an overnight fast, mice were given a single oral gavage of either chow slurry or fast food slurry and the cecum was harvested exactly 4 h later for 16S rRNA sequencing. (**A**) Shannon alpha diversity estimates for all six groups. Statistical analysis was performed via ANOVA. Comparisons within diet, across microbiome status are shown to the left (Cecum), and comparisons between food types are shown on the right (Diet). (**B**) NMDS plots based on the Bray-Curtis index between the chow and fast food cecal contents as well as the microbial composition of the food itself. Statistical analysis was performed with PERMANOVA, and *p*-values are labeled in plots. R^2 values are noted for comparisons with significant *p*-values and stand for percentage variance explained by the variable of interest. (**C**) Stacked bar charts of relative abundance (left y-axis) of the top 20 genera assembled across all six groups. Pairwise differential abundance analyses between (**D**) Chow Cecum and Chow Cecum Antibiotics, (**E**) Fast Food Cecum and Fast Food Cecum Antibiotics, (**F**) Chow Cecum and Fast Food Cecum, (**G**) Chow Cecum Antibiotics and Fast Food Cecum Antibiotics groups. Statistical analysis was performed with White's non-parametric *t*-test (*p*-values are labeled in plots). Con = control; Abx = antibiotics. *n* = 6–7 per group.
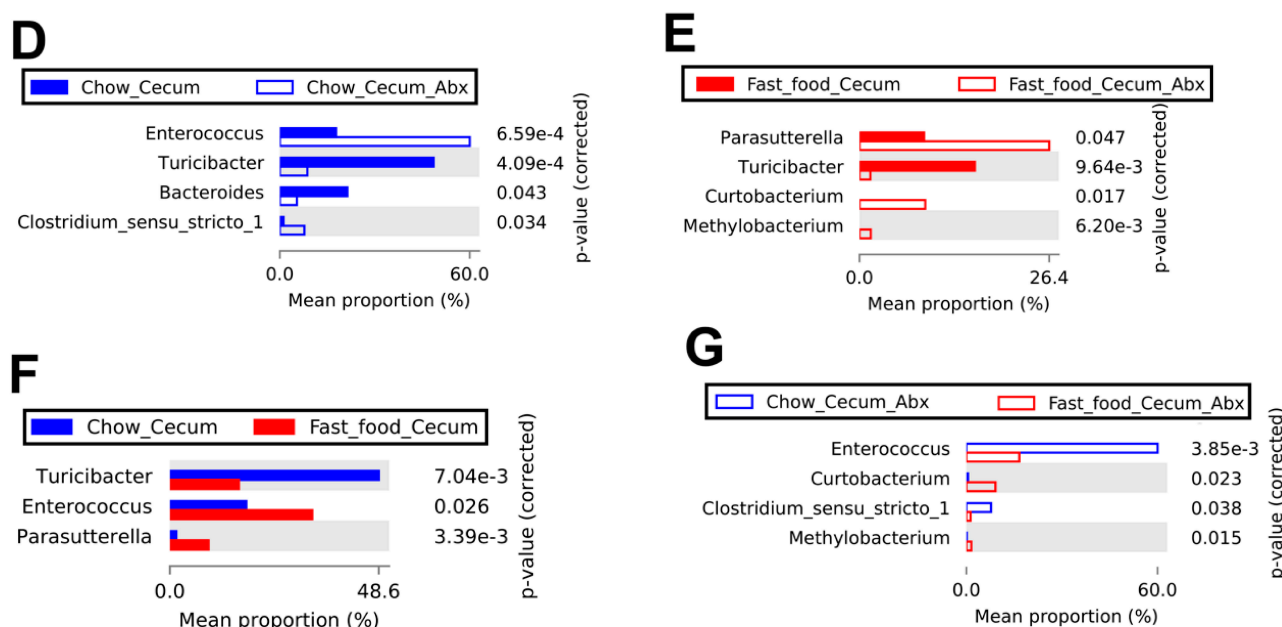
D

Chow_Cecum   Chow_Cecum_Abx

Enterococcus	6.59e-4
Turicibacter	4.09e-4
Bacteroides	0.043
Clostridium_sensu_stricto_1	0.034

0.0   60.0
Mean proportion (%)
p-value (corrected)

E

Fast_food_Cecum   Fast_food_Cecum_Abx

Parasutterella	0.047
Turicibacter	9.64e-3
Curtobacterium	0.017
Methylobacterium	6.20e-3

0.0   26.4
Mean proportion (%)
p-value (corrected)

F

Chow_Cecum   Fast_food_Cecum

Turicibacter	7.04e-3
Enterococcus	0.026
Parasutterella	3.39e-3

0.0   48.6
Mean proportion (%)
p-value (corrected)

G

Chow_Cecum_Abx   Fast_food_Cecum_Abx

Enterococcus	3.85e-3
Curtobacterium	0.023
Clostridium_sensu_stricto_1	0.038
Methylobacterium	0.015

0.0   60.0
Mean proportion (%)
p-value (corrected)

Figure 2. *Cont.*

In control water chow-gavaged mice, there was a significant enrichment of the *Turicibacter* and *Bacteroides* genera and loss of the *Enterococcus* and *Clostridium* genera when compared to the chow antibiotic treated group (Figure 2D). In control water fast food-gavaged mice, the genus *Turicibacter* was significantly enriched when compared to the fast food antibiotic treated group whereas the *Parasutterella, Curtobacterium,* and *Methylobacterium* genera were the most differentially abundant in the antibiotic treated group albeit these genera comprise a small proportion of the whole (Figure 2E). Notably, with an intact microbiome (non-antibiotic treated), *Turicibacter* was more abundant in chow-gavaged mice whereas *Enterococcus* and *Parasutterella* were enriched in fast food-gavaged mice (Figure 2F). Notably, some strains of *Turicibacter* produce lactic acid—a mediator of intestinal epithelial cell homeostasis [46,47]. Comparing chow- to fast food-gavaged mice in the context of antibiotic ablation, an enrichment of *Enterococcus*, which can act as an opportunistic pathogen [48], and *Clostridium* genera was observed (Figure 2G). Conversely, two environmental bacteria, *Methylobacterium* and *Curtobacterium,* were enriched in antibiotic ablated mice receiving fast food compared to chow (Figure 2G). These microbes have been described as members of complex biofilms in a variety of contexts ranging from nosocomial infections to plant pathogenesis [49,50]. In summary, these data suggest that a single meal equivalent of fast food is sufficient to remodel the gut microbial community structure in a short timeframe when compared to a chow control meal.

A Single Fast Food Meal Alters the Portal Blood Metabolome in a Gut Microbe-Dependent Manner

One of the key goals of this project was to unbiasedly identify gut microbe-associated postprandial metabolite alterations driven by a single fast food meal equivalent. To achieve this we performed untargeted

metabolomics in postprandial portal (i.e., the blood draining the gut) and peripheral plasma samples in mice either treated with or without broad spectrum antibiotics. The plasma untargeted metabolomics data in negative (Figure 3) and positive (Supplementary Figure S2) ESI modes were organized in eight distinct groups characterized by site of blood collection (portal versus peripheral), administration of control versus antibiotic water, and chow versus fast food meal gavage (Figure 3A). MetaboLyzer [20] was used to perform a single two-way comparison between portal plasma from chow- versus fast food-gavaged mice with an intact gut microbiome (non-antibiotic treated). Principal component analysis demonstrated strong separation between groups in both the negative (Figure 3B) and positive (Supplementary Figure S2B) ESI modes. KEGG pathway analysis identified differences in putative metabolites related to unsaturated fatty acid biosynthesis and arachidonic acid metabolism, as well as amino acid metabolism in the negative ESI mode (Figure 3C). A parallel analysis of positive ESI mode ions corroborated the significant difference in putative lipid biosynthesis metabolites resulting from the fast food meal (Supplementary Figure S2C).

In a separate analysis using an in-house developed algorithm (Supplementary File S3), several two-group analyses were performed simultaneously in an attempt to focus on fast food-driven metabolites that also have gut microbe-associated patterns i.e., metabolites that were simultaneously enriched in portal blood, suppressed by antibiotic, and altered by fast food feeding (Figure 3D). In the negative ESI mode, 3829 ions met the presence-threshold with greater than 50% of samples reporting a non-zero value and were subsequently analyzed. Multiple two-way comparisons were made to identify ions of significantly greater intensity within the portal blood of control water fast food-gavaged mice when compared to each of the following: portal blood of control water chow-gavaged mice, portal blood of all antibiotic water treated mice, and all peripheral blood samples (Figure 3E–G, comparison bars). Overall, 463 ions met all criteria, including 138 with putative database identifications (Figure 3D). All 463 ions were scored based on the fold-change differences between groups of each comparison to rank their fitness of the multiple criteria listed. The ion with reported mass-to-charge ratio_retention time (m/z_RT) of 423.2919_11.3959 was highly scored and later structurally confirmed to be 18:0 LPA (Figure 3E). Many other putatively identified (Figure 3F) and unidentified (Figure 3G) ions were also highly scored and fit the multiple criteria well (Supplementary Figure S2E–G). A parallel analysis was performed for the positive ESI mode (Supplementary Figure S2), and many additional highly scored ions closely following a dual fast food-driven gut microbe-associated pattern were identified. Data and results generated from both negative and positive ESI modes are available in Supplementary File S1. Remarkably, in the negative ESI mode, nearly all (1903 out of 1991) metabolites that were significantly higher in portal versus peripheral blood were also significantly higher in the portal blood of control water versus

antibiotic water (Figure 3D). In other words, nearly all portal-blood enriched metabolites were gut-microbe dependent. This demonstrates the immense importance of the gut microbiome to the portal vein niche, and also the importance of portal blood collection in study of the gut microbiome.
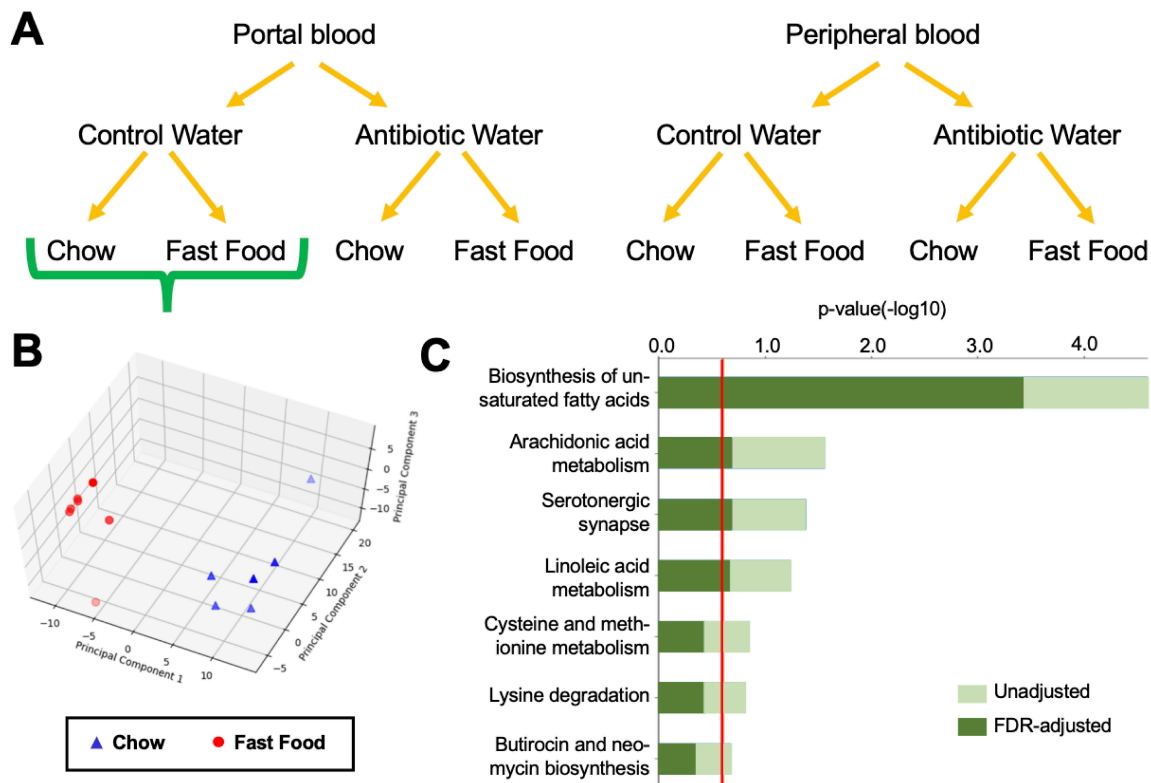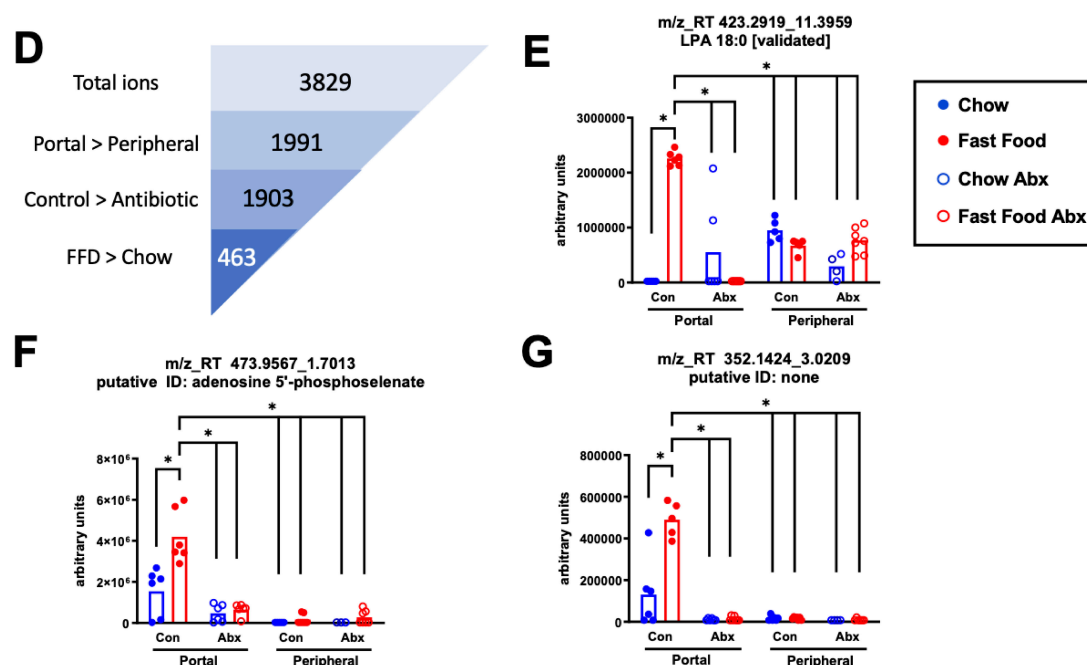

Figure 3. A Single Fast Food Meal Alters the Portal Blood Metabolome in a Gut Microbe-Dependent Manner. (**A**) 6-week old male C57BL6/J mice were randomly assigned to control drinking water or drinking water supplemented with broad spectrum antibiotics for two weeks. Following an overnight fast, mice were given a single oral gavage of either chow slurry or fast food slurry and sacrificed exactly 4 h later. Portal and peripheral blood were taken for plasma and LCMS-based untargeted metabolomics was performed in the negative ESI mode. (**B**) PCA and (**C**) KEGG pathway analysis of portal blood from chow versus fast food gavage of control water mice generated using MetaboLyzer. (**D**) Multiple two-group comparisons were made to identify ions enriched within the portal blood that were greater in the control water, fast food gavage group. 463 ions satisfy all criteria. (**E**) The comparison tests performed are shown with overlying horizontal comparison bars. Ion mass charge_retention time (*m*/z_RT) 423.2819_11.3959 satisfied all criteria and was structurally validated as 18:0 LPA. (**F**) Ion *m*/z_RT 473.9567_1.7013 satisfies all criteria and is putatively identified as adenosine 5'phosphoselenate. (**G**) Ion *m*/z_RT 342.1424_3.0209 satisfies all criteria but does not have a putative identification. *$q < 0.10$ (Mann-Whitney *U* test). Con = control; Abx = antibiotics. n = 4–7 per group.

Figure 3. *Cont.*

A Single Fast Food Meal Alters the Hepatic Metabolome in a Gut Microbe-Dependent Manner

To understand diet-microbe-host driven alterations in the hepatic metabolome, we performed a quantitative targeted metabolomic panel in livers isolated 4 h after a fast food meal. This targeted assay included structurally diverse metabolite classes including amino acids, biogenic amines, monosaccharides, glycerophospholipids, and neutral lipids. We generated heatmap plots to highlight metabolite differences between livers from chow and fast food meal gavage groups of mice with an intact microbiome (Figure 4A left side). These differences were not maintained in mice that had their microbiota ablated by prior administration of antibiotics in the drinking water (Figure 4A right side), implicating the role of an intact gut microbial metabolism on a meal-specific liver metabolome. When considering the top 50 differentially detected liver metabolites across gut microbiome status within the chow-gavaged group (Supplementary Figure S3A left side), some of these differences were maintained in fast food-gavaged mice (Supplementary Figure S3A right side). Similarly, differences across the gut microbiome status within the fast food-gavaged group (Supplementary Figure 3B left side) were only slightly maintained in chow-gavaged mice (Supplementary Figure S3B right side). Taken together, this suggests that antibiotic-mediated differences in the hepatic metabolome were present in both chow and fast food meal groups, though the particular differences were diet-specific.
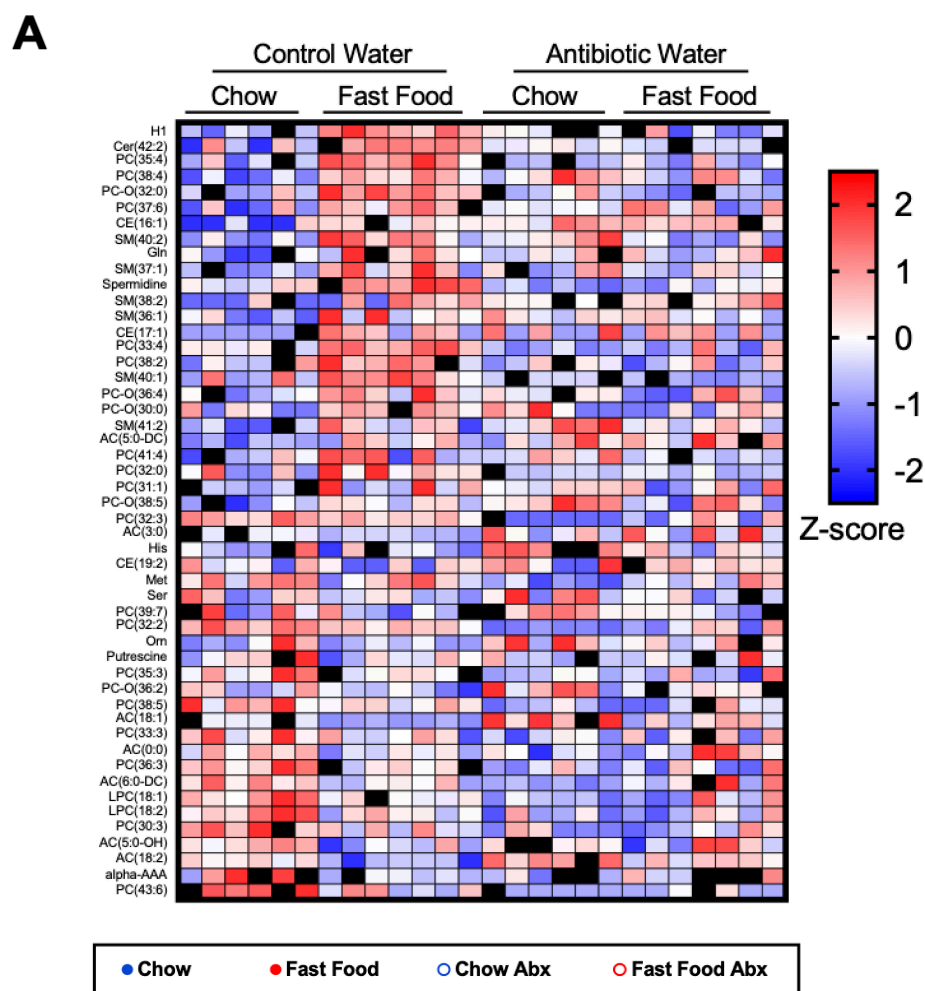
Figure 4. A Single Fast Food Meal Alters the Hepatic Metabolome in a Gut Microbe-Dependent Manner. 6-week old male C57BL6/J mice were randomly assigned to control drinking water or drinking water supplemented with broad spectrum antibiotics for two weeks. Following an overnight fast, mice were given a single oral gavage of either chow slurry or fast food slurry and the liver was harvested exactly 4 h later for targeted metabolomics. (**A**) Heatmap of the top 50 differentially expressed molecules within drinking water type, across diet. Groups listed above with samples contained within columns; row metabolite identification listed on left; z-score normalized values scaled by row (red = increase, blue = decrease, black = missing value or excluded outlier). (**B**) AC(18:1) and AC(18:2) demonstrate diet-driven changes in both control and antibiotic-treated mice. (**C**) PC(32:1) and AC(2:0) demonstrate antibiotic-driven changes in both chow and fast food diet gavage mice. (**D**) Spermidine and the hexose monosaccharides have dual diet- and antibiotic-driven changes, appearing highest in the fast food diet control water group. *$q < 0.15$, **$q < 0.05$ (Mann-Whitney U test). Abx = antibiotics; H1 = hexose monosaccharides; Cer = ceramide; PC = phosphatidylcholine; CE = cholesteryl ester; SM, sphingomyelin; AC = acylcarnitine; LPC = lysophosphatidylcholine; alpha-AAA = alpha-aminoadipic acid. n = 6–7 per group.
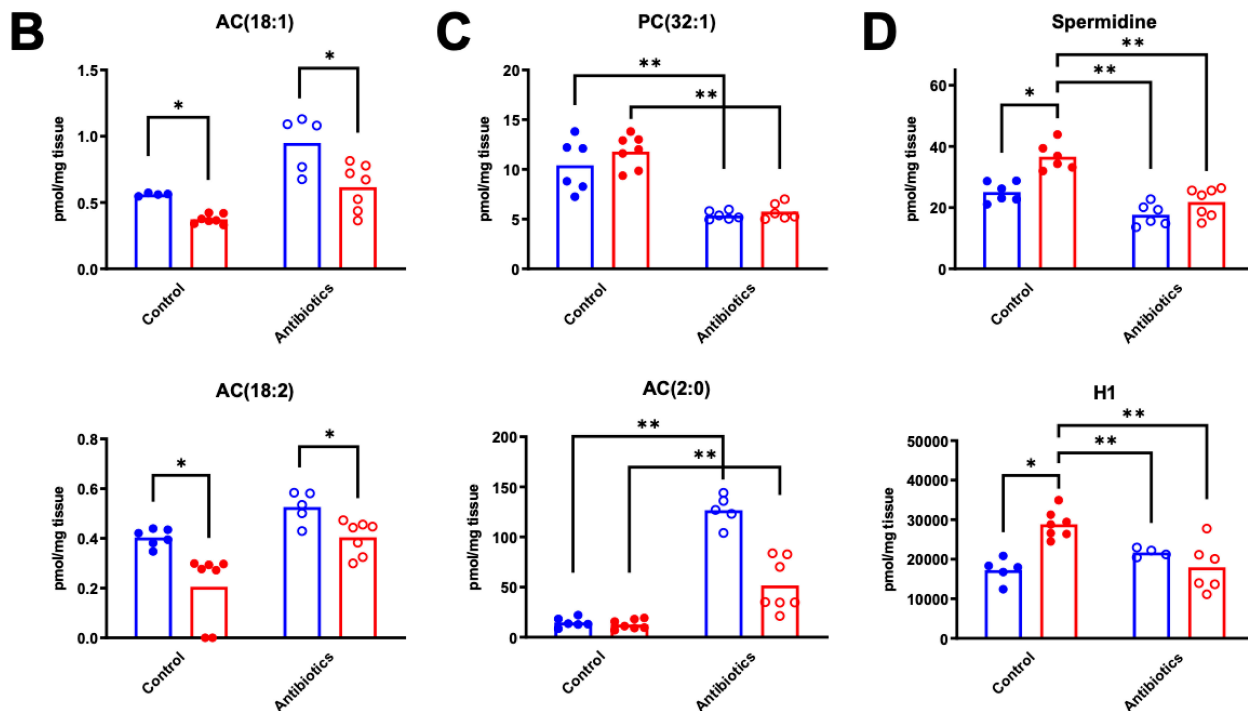
Figure 4. *Cont.*

Additional comparisons across meals and microbiome status identified commonly occurring molecules that warrant further investigation. For example, the 18:1 and 18:2 acylcarnitine species vary significantly across meals, irrespective of an intact microbiome (Figure 4B). When comparing across gut microbiome status, 32:1 phosphatidylcholine and 2:0 acylcarnitine (Figure 4C), and triglycerides (Supplementary Figure S4) vary significantly for both meal types. Analogous to our plasma untargeted metabolomics analysis above (Figure 3D), metabolites dually dependent on fast food and the microbiome were sought after. Spermidine, an aliphatic polyamine compound, and the hexose monosaccharides demonstrated dual diet- and microbiome-driven changes, appearing highest in the control water fast food-gavaged group (Figure 4D). Together, this suggests that gut microbiome status has a larger influence on liver metabolites than meal type.

A Single Fast Food Meal Rapidly Alters Hepatic Gene Expression in a Gut Microbe-Dependent Manner

Given the marked portal blood metabolite signatures as well as the unique diet- and gut microbiota-dependent hepatic metabolome changes, we next aimed to understand the potential impact of a human relevant fast food meal on the host. We used an unbiased RNA sequencing approach to profile acute postprandial transcriptomic changes within the liver (Figure 5). Distinct diet- and gut microbiota-dependent clustering was apparent after NMDS analysis (Figure 5A). For mice with an intact gut microbiome, there were notable differences between the hepatic

transcriptome of chow-gavaged and fast food-gavaged mice (Figure 5B). Importantly, these unique profiles were not retained in the microbiome ablated cohort suggesting a strong gut microbial dependency (Figure 5B–D), in agreement with the liver metabolomics results (Figure 4A). We observed an upregulation of *Fmo3* encoding the enzyme responsible for conversion of TMA to TMAO in fast food fed mice on control drinking water, which could be related to the red meat component of fast food [8–10]. Pathway analysis revealed a surprising fast food-induced dysregulation of circadian rhythmicity associated genes (Figure 5E). These data were further corroborated using RT-qPCR where it was observed that the relative mRNA expression of Cryptochrome 1 (*Cry1*), a key repressor of the core circadian oscillator complex (Figure 5F) and Circadian Associated Repressor of Transcription (*Ciart*), a core clock-independent repressor (Figure 5G) are markedly upregulated upon consumption of a fast food meal in mice harboring an intact gut microbiome. Importantly, the transcriptional upregulation of these core clock dependent and independent circadian repressors was not observed in mice who consumed a fast food meal with an antibiotic ablated microbiome. Taken together, these data reveal rapid postprandial hepatic transcriptional changes that are strongly dependent on the diet with a possible gut microbial contribution.

The complex relationship between diet composition and the gut microbiome is an attractive target in the study of metabolic syndrome (MetS) and cardiovascular disease. Unfortunately, the vast majority of animal studies in this area study cardiometabolic phenotypes in the context of diets that have no relevance to what humans actually eat. For example, rodent chow is not standardized and changes according to raw materials available for animal food production, which changes seasonally. Even carefully formulated synthetic rodent diets such as the chemically-defined chow used here, or popular high fat or Western diets, do not accurately mimic the micronutrient and macronutrient content of common human diets. To overcome this, we instead provided a single human relevant fast food meal to mice with or without antibiotic-mediated suppression of the gut microbiome to understand the meta-organismal metabolomic signatures that arise after fast food dietary substrates are presented. The main findings of this study demonstrate that consumption of a single fast food meal: (1) rapidly alters the gut microbiome in a way that is not predicted by the microbes present in the fast food meal, (2) rapidly alters the portal and peripheral plasma metabolome in a microbiome-dependent manner, (3) rapidly alters the host hepatic transcriptome and metabolome in a microbiome-dependent manner, and (4) rapidly alters the expression of hepatic genes related to circadian dysregulation in a microbiome-dependent manner. Collectively, these data provide a glimpse into microbe-host interactions when relevant dietary substrates are provided, and bolster the concept that many host

transcriptional and metabolic alterations fueled by consumption of fast food are shaped by the gut microbial endocrine organ [51].
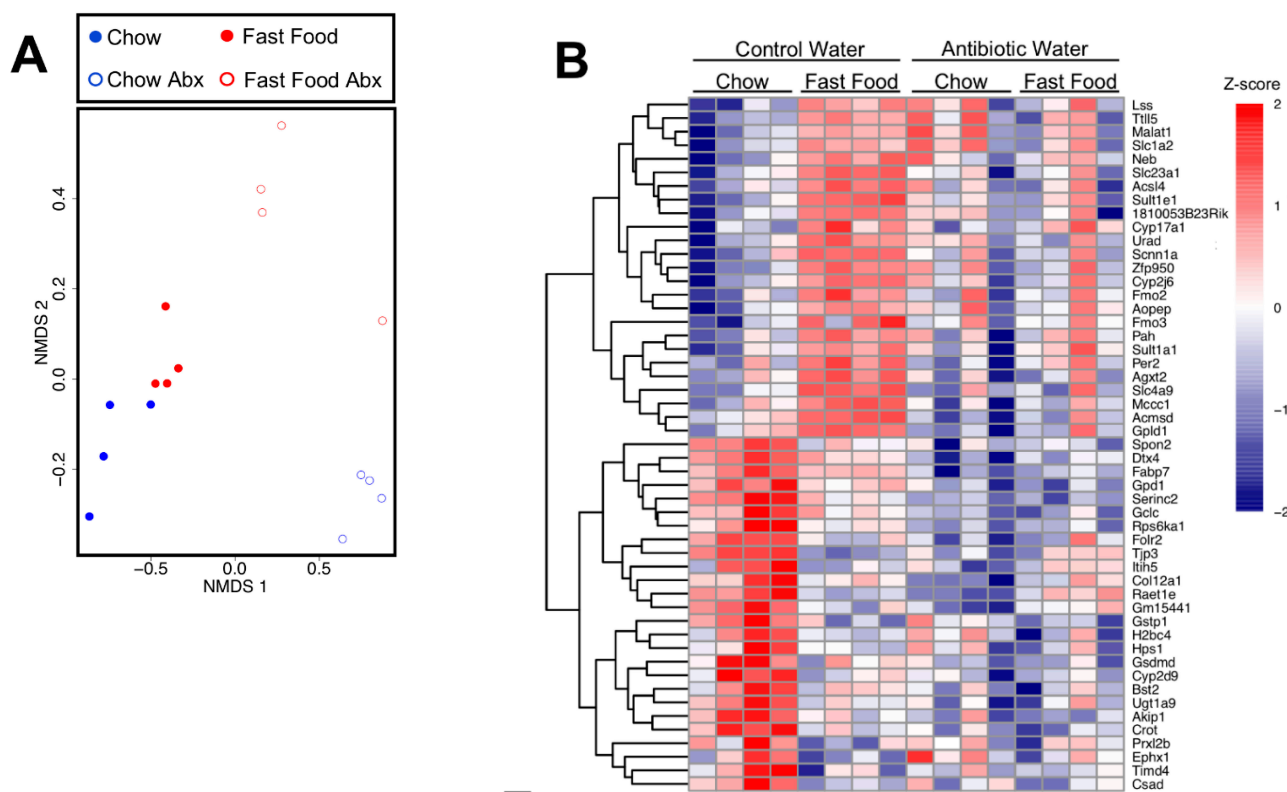

Figure 5. **A Single Fast Food Meal Rapidly Alters Hepatic Gene Expression in a Gut Microbe-Dependent Manner.** 6-week old male C57BL6/J mice were randomly assigned to control drinking water or drinking water supplemented with broad spectrum antibiotics for two weeks. Following an overnight fast, mice were given a single oral gavage of either chow slurry or fast food slurry and the liver was harvested exactly 4 hours later for bulk RNA sequencing. (**A**) NMDS of RNA-Seq transcriptome data representing the hepatic gene expression signature of the top 500 differentially expressed transcripts as sorted by log2 fold change between chow (blue) and fast food (red) in the absence (filled dots) or presence (hollow dots) of antibiotics. The NMDS was performed using DESeq2 normalized counts. (**B**) Heatmap of hierarchically clustered differentially expressed genes arranged by adjusted p-value and log2 fold change. *Z*-score normalized values scaled by row. (**C**) Volcano plot of RNA-Seq transcriptome data representing hepatic gene expression signature of chow control water mice to fast food control water mice. (**D**) Volcano plot of RNA-Seq transcriptome data representing hepatic gene expression signature of chow antibiotic water mice to fast food antibiotic water mice. Genes highlighted in red correspond to those that are significantly differentially expressed (adjusted $p < 0.001$) with a log2 fold change >1.5. (**E**) Parent gene ontology assignments of the top 150 differentially expressed genes as sorted by adjusted *p*-value between chow control water and fast food control water mice. $n = 4$ per group for all RNASeq analysis. (**F–G**) qPCR validation of differentially expressed circadian repressor genes revealed by RNA-Seq. Statistical analysis of qPCR data was performed using a two-way ANOVA with Tukey's multiple comparison test where * $p < 0.05$, ** $p < 0.01$, *** $p < 0.001$, **** $p < 0.0001$. $n = 6–7$ for all qPCR analysis. Abx = antibiotics; NS = not significant; FC = fold change.
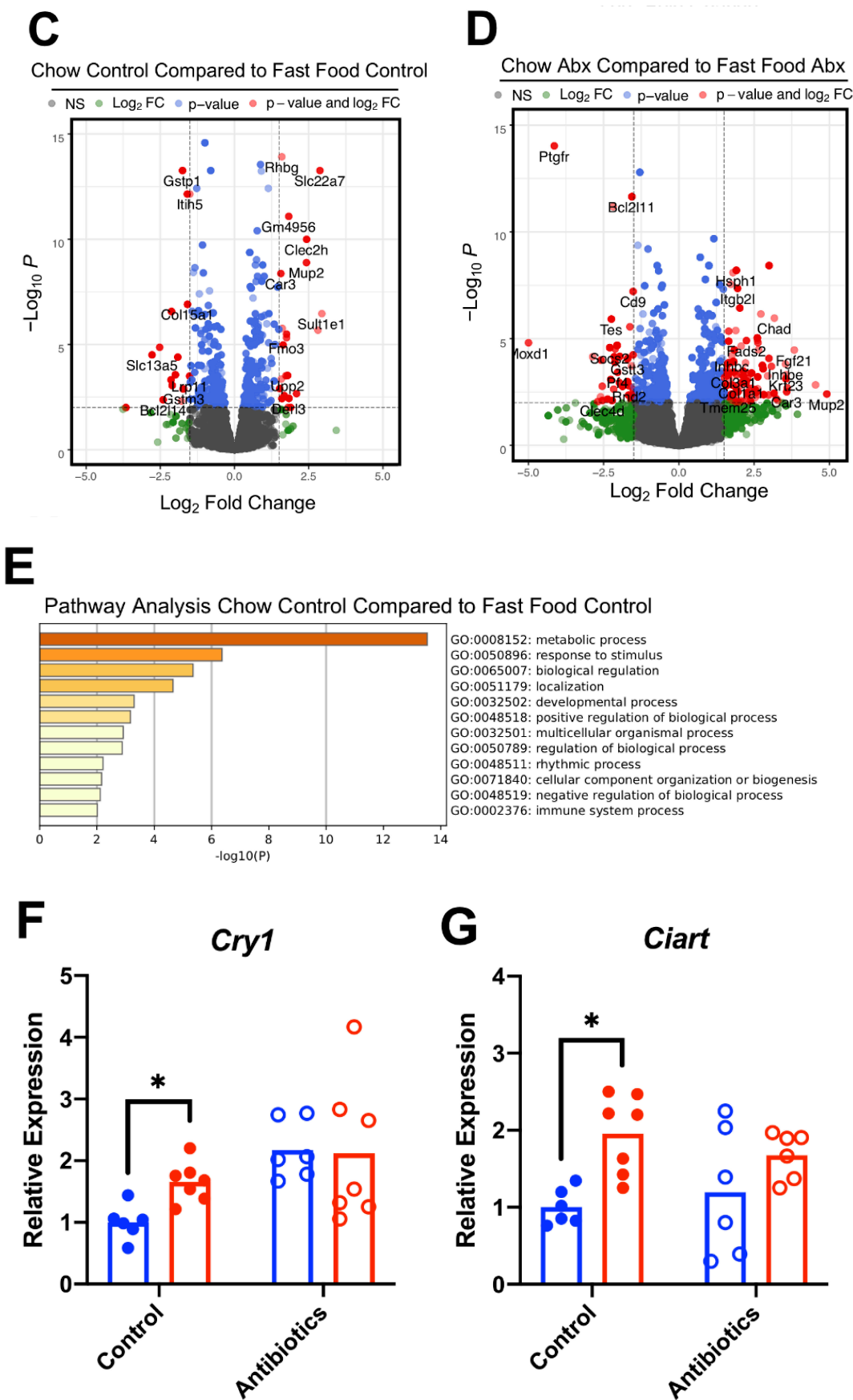
Figure 5. *Cont.*

DISCUSSION

The past decade has seen an explosion of research associating the relative abundance of gut microbes to human disease, relying on classic 16S ribosomal RNA approaches or more recently by metagenomic deep sequencing. Large collaborative microbiome-focused research consortia have leveraged such methodology to catalogue the types of bacteria resident in the human intestine, and have shown that gut microbiome structure can be dynamically altered by several variables including diet, age, host genetics, and antibiotic exposure [52–54]. Among all of the environmental factors that impact gut microbiome structure, diet is clearly a major determinant shaping community structure and function [41–43]. Although it is well appreciated that diet can profoundly alter the gut microbiome, most studies to this point have focused on effects that occur after days or weeks on dietary intervention. Here, we show that a single human-relevant fast food meal can rapidly reorganize gut microbiome communities in mice. Strikingly, just 4 h after fast food consumption, gut microbiome shifts were observed that were largely independent of the microbial sequences that originated from the diets (Figure 2). For example, commensal food-associated bacteria such as *Lactobacillus, Lactococcus, and Streptococcus* were the most abundant genera in the fast food meal itself, yet these taxa did not contribute to remarkable shifts in the cecal microbiota of fast food gavaged mice. This highlights that the shifts in cecal microbiome composition are in response to dietary constituents rather than caused by background microbes that were present in the food. Although some of the observed differences in gut microbial community composition are consistent with previous findings, such as the negative association of *Turicibacter* with high-fat feeding [55–57] or positive association of *Enterococcus* with obesity [58], these data should be cautiously interpreted due to their correlative and often discrepant nature [59]. In mice with an intact gut microbiome (that were receiving control drinking water prior to gavage), the administration of a fast food gavage led to changes in cecal microbial content, with notable increases in the pathobiont *Enterococcus* and *Parasutterella*, while the opposite was seen in antibiotic water treated groups. Interestingly, a striking increase in *Burkholderia/Paraburkholderia* was observed in the fast food antibiotic water group, likely due to the proliferation of antibiotic-resistant colonizers. These data, coupled with many other recent published reports, support the notion that a single meal can have profound effects gut microbiome community structure [60,61].

It is clear that consumption of key dietary substrates can shape the types of bacteria that are present in the intestine, but less is understood about the complex interplay between dietary substrate availability, gut microbe-derived metabolite production, and downstream co-metabolism driven by the host. The use of LCMS-based metabolomics has become a powerful tool in the study of human health and disease, particularly in identifying meta-organismal nutrient metabolism pathways [62–66]. Here

we used an untargeted metabolomics platform as an unbiased approach to identify gut microbe-derived metabolites that are produced postprandially after a human-relevant fast food meal. We focused our efforts on postprandial metabolites that were enriched in the portal circulation, given that many microbe-derived metabolites are rapidly converted to secondary metabolites in the host liver. The untargeted metabolomics platform we used here is only able to structurally predict <10% of the metabolites detected, and further structural validation is needed for each putative spectral feature in the dataset. To aid with future investigation of diet-microbe-host metabolomic data, we have generated a computer program using Python coding language to perform multigroup analyses and identify metabolites meeting a particular distribution profile (Supplementary File S3). Multiple criteria were fed into this program to identify fast food-altered and gut microbe-dependent metabolites (Figure 3D-G). Although we were not able to structurally identify all microbiota-associated fast food-driven metabolites, we did confirm one such metabolite as 18:0 lysophosphatidic acid (LPA) which increases preferentially in the portal blood of mice provided fast food substrate, yet this fast food-induced spike is suppressed by antibiotic treatment (Figure 3E). The results shown for 18:0 LPA are consistent with its pharmacokinetic profile of undergoing rapid first-pass hepatic metabolism [67]. Interestingly, 18:0 LPA has previously been associated with liver dysfunction and cardiovascular disease [68,69]. A number of other putatively identified metabolites were found to match this distribution profile, and their information listed in Supplementary File S1. Although beyond the scope of this work, further structural identification of other fast food-derived gut microbial metabolites identified here has the potential to provide new links between fast food, the gut microbial endocrine organ, and human disease.

In addition to performing untargeted metabolomics in the circulation, we also set out to understand the transcriptomic and metabolomic alterations driven by a fast food meal in the host liver. Quantitative targeted metabolomics was performed to detect molecular species of key metabolite classes including amino acids, biogenic amines, carbohydrates, acyl-carnitines, polar lipids, and neutral lipids. The diet- and antibiotic-driven liver lipid profiles (Supplementary Figure S4) and liver metabolite profiles (Figure 4) varied significantly between meal type just four hours after gavage, though a larger effect was seen as a result of antibiotic administration (Supplementary Figure S3). Spermidine levels varied both in a diet- and microbe-dependent manner, appearing highest in livers of the control water fast food group. Spermidine is an aliphatic polyamine compound that is obtained from diet, synthesized endogenously, or produced by intestinal bacteria [70] and has been associated with a number of positive physiologic effects such as increasing lifespan as well as negative pathologic effects such as tumorigenesis [71,72]. Its expression pattern, appearing higher in fast food mice with an intact microbiome

compared to their antibiotic treated counterparts, implicates the induction of host de novo biogenesis or alterations of spermidine-producing gut microbes in response to a fast food meal.

In an effort to determine the putative impact of these portal blood and hepatic metabolites on the host, an unbiased RNA-sequencing approach was used to profile the liver transcriptome. In the control water groups, there was a marked difference in gene expression between meal types (Figure 5B left side), though these diet-driven changes were not seen in the antibiotic water groups (Figure 5B right side), implicating the gut microbiome in diet-driven host transcriptional changes. This pattern was congruent with the liver metabolomics results (Figure 4A left side, 4A right side), further supporting a possible gut microbial contribution. The expression of flavin-containing monooxygenase 3 (*Fmo3*), encoding the enzyme responsible for converting gut microbe-derived trimethylamine (TMA) to its heart disease-associated co-metabolite trimethylamine-*N*-oxide (TMAO), was found to be higher in the fast food group compared to chow group of mice with an intact microbiome. As expected, the fast food meal did not promote an increase in *Fmo3* expression in the antibiotic treated groups. This is yet another example whereby the expression of *Fmo3* is altered in mouse models of progressive cardiometabolic disease [73–76]. Of note, consumption of a fast food meal promoted hepatic transcription of several circadian repressors, but only in mice with an intact gut microbial community (Figure 5B,E–G). These data coincide with the collective understanding that diet can influence circadian rhythmicity and in the case of high fat and Western diets, cause marked disruption of circadian oscillatory programs [77–79]. Moreover, the gut microbial contribution to host circadian rhythmicity and metabolism has been established in recent years, underscoring the complexity of microbe-host interactions [80,81]. Collectively, this study utilized a multi-omics approach to study the interrelationship between varying diets and the gut microbiome to gain novel insights toward MetS and cardiovascular disease. The multi-omic data generated here can be used as a lens to focus further investigation into mechanisms by which fast food diets promote cardiometabolic disease.

CONCLUSIONS

Herein, we have leveraged a multi-omics approach to identify microbial metabolites produced postprandially from a single fast food meal. This approach differs from conventional rodent models of MetS by introducing a single meal equivalent that more closely recapitulates a human Western diet. Leveraging tools such as 16S rRNA gene sequencing, untargeted and targeted metabolomics, and host RNA sequencing, we uncovered distinct diet- and gut microbe-dependent metabolites and their associated impact on the hepatic transcriptome. Important to note, limitations of this study include but are not limited to the fact that

antibiotic ablation does not completely eliminate the gut bacterial community and has been reported to reduce dietary lipid absorption in rats and mice [82,83]. The use of germ-free mice would offer a more rigorous method to study the microbial aspect in terms of metabolites and ruling out hepatic transcriptional changes due to the antibiotics themselves. However, there are caveats to using germ-free mice, as they are known to have underdeveloped immune systems [84–86]. Moreover, studying the mouse microbiome with human relevant diet is limiting and it may be more appropriate to study a mouse colonized with a human derived microbiome, although this approach has its own limitations [84]. Finally, murine fat metabolism differs from the human condition such that mice lack cholesterol ester transfer protein (CETP) and have divergent lipoprotein profiles compared to humans, potentially limiting the translational relevance of the findings reported herein. Our data suggest that following the consumption of a single human-relevant fast food meal, unique diet- and gut microbe-dependent metabolites are detected in addition to rapid transcriptional reprogramming of the liver. Further investigation is warranted to determine if these metabolites are causally linked to host transcriptional changes and the development or progression of MetS.

DATA AVAILABILITY

The datasets generated from (or analyzed in) the study can be found in the supplementary files or have been deposited in NCBI's Gene Expression Omnibus [34] and are accessible through GEO Series accession number GSE165756.

SUPPLEMENTARY MATERIALS

The supplementary materials are available online at https://doi.org/10.20900/immunometab20210029.

Supplementary Figure S1. Bomb calorimetry of dietary slurries used for gavage.

Supplementary Figure S2. Plasma metabolomic signatures – positive ionization mode.

Supplementary Figure S3. Hepatic phospholipid analysis.

Supplementary Figure S4. Hepatic lipid analysis.

Supplementary File S1. Plasma untargeted metabolomics.

Supplementary File S2. Liver targeted metabolomics using AbsoluteIDQ® p400 HR kit from Biocrates Life Sciences AG.

Supplementary File S3. Python program used to analyze plasma untargeted metabolomics data.

Supplementary File S4. Python program used to analyze liver targeted metabolomics data.

Supplementary Table S1. Nutritional information for oral gavage slurry components.

Supplementary Table S2. Ingredients list for oral gavage slurry components.

AUTHOR CONTRIBUTIONS

LJO and JMB designed the study. LJO, AK, and ADG performed the mouse experiments. DO, RB, ALB, TDM, BBW, and MG performed all mass spectrometry and subsequent analysis. NS performed the analysis of 16S rRNA sequencing data. PL and GAMC compiled the nutritional information for each diet. LJO, DO, JC, and JMB analyzed the data. LJO, DO, JC, and JMB wrote the paper with input from all authors.

CONFLICTS OF INTEREST

The authors declare that they have no conflicts of interest.

REFERENCES

1.   Moore JX. Metabolic Syndrome Prevalence by Race/Ethnicity and Sex in the United States, National Health and Nutrition Examination Survey, 1988–2012. Prev Chronic Dis. 2017;14:E24.
2.   Saklayen MG. The Global Epidemic of the Metabolic Syndrome. Curr Hypertens Rep. 2018;20(2):12.
3.   Mottillo S, Filion KB, Genest J, Joseph L, Pilote L, Poirier P, et al. The metabolic syndrome and cardiovascular risk a systematic review and meta-analysis. J Am Coll Cardiol. 2010 Sep 28;56(14):1113-32.
4.   Koeth RA, Lam-Galvez BR, Kirsop J, Wang Z, Levison BS, Gu X, et al. L-Carnitine in omnivorous diets induces an atherogenic gut microbial pathway in humans. J Clin Invest. 2019 Jan 2;129(1):373-87.

5.   Wang Z, Bergeron N, Levison BS, Li XS, Chiu S, Jia X, et al. Impact of chronic dietary red meat, white meat, or non-meat protein on trimethylamine *N*-oxide metabolism and renal excretion in healthy men and women. European Heart Journal. 2019 Feb 14;40(7):583-94.

6.   Cassidy A, Minihane A-M. The role of metabolism (and the microbiome) in defining the clinical efficacy of dietary flavonoids. Am J Clin Nutr. 2017 Jan;105(1):10-22.

7.   Rechner AR, Smith MA, Kuhnle G, Gibson GR, Debnam ES, Srai SKS, et al. Colonic metabolism of dietary polyphenols: influence of structure on microbial fermentation products. Free Radic Biol Med. 2004 Jan 15;36(2):212-25.

8.   Wang Z, Klipfell E, Bennett BJ, Koeth R, Levison BS, DuGar B, et al. Gut flora metabolism of phosphatidylcholine promotes cardiovascular disease. Nature. 2011 Apr 7;472(7341):57–63.

9.   Tang WHW, Wang Z, Levison BS, Koeth RA, Britt EB, Fu X, et al. Intestinal Microbial Metabolism of Phosphatidylcholine and Cardiovascular Risk. N Engl J Med. 2013 Apr 25;368(17):1575-84.

10. Koeth RA, Wang Z, Levison BS, Buffa JA, Org E, Sheehy BT, et al. Intestinal microbiota metabolism of L-carnitine, a nutrient in red meat, promotes atherosclerosis. Nat Med. 2013 May;19(5):576-85.

11. Schugar RC, Willard B, Wang Z, Brown JM. Postprandial gut microbiota-driven choline metabolism links dietary cues to adipose tissue dysfunction. Adipocyte. 2017 Nov 27;7(1):49-56.

12. Boutagy NE, Neilson AP, Osterberg KL, Smithson AT, Englund TR, Davy BM, et al. Short-term high-fat diet increases postprandial trimethylamine-*N*-oxide in humans. Nutr Res. 2015 Oct;35(10):858-64.

13. Caporaso JG, Kuczynski J, Stombaugh J, Bittinger K, Bushman FD, Costello EK, et al. QIIME allows analysis of high-throughput community sequencing data. Nat Methods. 2010 May;7(5):335-6.

14. Callahan BJ, McMurdie PJ, Rosen MJ, Han AW, Johnson AJA, Holmes SP. DADA2: High-resolution sample inference from Illumina amplicon data. Nat Methods. 2016 Jul;13(7):581-3.

15. McMurdie PJ, Holmes S. phyloseq: an R package for reproducible interactive analysis and graphics of microbiome census data. PLoS One. 2013;8(4):e61217.

16. McMurdie PJ, Holmes S. Waste not, want not: why rarefying microbiome data is inadmissible. PLoS Comput Biol. 2014 Apr;10(4):e1003531.

17. Wickham H. ggplot2: Elegant Graphics for Data Analysis. New York (USA): Springer Publishing Company; 2009.

18. Benjamini Y, Hochberg Y. Controlling the False Discovery Rate: A Practical and Powerful Approach to Multiple Testing. J R Stat Soc Series B. 1995;57(1):289-300.

19. Tiit E-M. Nonparametric Statistical Methods. Myles and Douglas A. Wolfe, Wiley; 1999. No. of pages: xiii+779. Price: £ 39.95. ISBN 0-471-19045-4. Stat Med. 2000;19(10):1386-8.

20. Mak TD, Laiakis EC, Goudarzi M, Fornace AJ. MetaboLyzer: A Novel Statistical Workflow for Analyzing Post-Processed LC/MS Metabolomics Data. Anal Chem. 2014 Jan 7;86(1):506-13.

21. Yekutieli D, Benjamini Y. Resampling-based false discovery rate controlling multiple test procedures for correlated test statistics. J Stat Plan Inference. 1999 Dec 1;82(1):171-96.

22. Kanehisa M, Goto S. KEGG: Kyoto Encyclopedia of Genes and Genomes. Nucleic Acids Res. 2000 Jan 1;28(1):27-30.

23. Wishart DS, Jewison T, Guo AC, Wilson M, Knox C, Liu Y, et al. HMDB 3.0—The Human Metabolome Database in 2013. Nucleic Acids Res. 2013 Jan;41(Database issue):D801-7.

24. Sud M, Fahy E, Cotter D, Brown A, Dennis EA, Glass CK, et al. LMSD: LIPID MAPS structure database. Nucleic Acids Res. 2007 Jan;35(Database issue):D527-32.

25. Karp PD, Billington R, Caspi R, Fulcher CA, Latendresse M, Kothari A, et al. The BioCyc collection of microbial genomes and metabolic pathways. Brief Bioinform. 2019 Jul 19;20(4):1085-93.

26. Martin M. Cutadapt removes adapter sequences from high-throughput sequencing reads. EMBnet.journal. 2011 May 2;17(1):10-2.

27. Dobin A, Davis CA, Schlesinger F, Drenkow J, Zaleski C, Jha S, et al. STAR: ultrafast universal RNA-seq aligner. Bioinformatics. 2013 Jan 1;29(1):15-21.

28. Anders S, Pyl PT, Huber W. HTSeq—a Python framework to work with high-throughput sequencing data. Bioinformatics. 2015 Jan 15;31(2):166-9.

29. Love MI, Huber W, Anders S. Moderated estimation of fold change and dispersion for RNA-seq data with DESeq2. Genome Biol. 2014;15(12):550.

30. Kolde R. pheatmap: Pretty Heatmaps. 2019. Available from: https://CRAN.R-project.org/package=pheatmap. Accessed 2021 September 13.

31. Neuwirth E. RColorBrewer: ColorBrewer Palettes. 2014. Available from: https://CRAN.R-project.org/package=RColorBrewer. Accessed 2021 September 18.

32. Robinson MD, McCarthy DJ, Smyth GK. edgeR: a Bioconductor package for differential expression analysis of digital gene expression data. Bioinformatics. 2010 Jan 1;26(1):139-40.

33. Zhou Y, Zhou B, Pache L, Chang M, Khodabakhshi AH, Tanaseichuk O, et al. Metascape provides a biologist-oriented resource for the analysis of systems-level datasets. Nat Commun. 2019 Apr 3;10(1):1523.

34. Edgar R, Domrachev M, Lash AE. Gene Expression Omnibus: NCBI gene expression and hybridization array data repository. Nucleic Acids Res. 2002 Jan 1;30(1):207-10.

35. Brown JM, Betters JL, Lord C, Ma Y, Han X, Yang K, et al. CGI-58 knockdown in mice causes hepatic steatosis but prevents diet-induced obesity and glucose intolerance. J Lipid Res. 2010 Nov;51(11):3306-15.

36. Brown JM, Bell TA, Alger HM, Sawyer JK, Smith TL, Kelley K, et al. Targeted depletion of hepatic ACAT2-driven cholesterol esterification reveals a non-biliary route for fecal neutral sterol loss. J Biol Chem. 2008 Apr 18;283(16):10522-34.

37. Brown JM, Chung S, Sawyer JK, Degirolamo C, Alger HM, Nguyen T, et al. Inhibition of stearoyl-coenzyme A desaturase 1 dissociates insulin resistance and obesity from atherosclerosis. Circulation. 2008 Sep 30;118(14):1467-75.

38. Helsley RN, Venkateshwari V, Brown AL, Gromovsky AD, Schugar RC, Ramachandiran I, et al. Obesity-linked suppression of membrane-bound O-Acyltransferase 7 (MBOAT7) drives non-alcoholic fatty liver disease. eLife. 2019 Oct 17;8:e49882.

39. Gromovsky AD, Schugar RC, Brown AL, Helsley RN, Burrows AC, Ferguson D, et al. Δ-5 Fatty Acid Desaturase FADS1 Impacts Metabolic Disease by Balancing Proinflammatory and Proresolving Lipid Mediators. Arterioscler Thromb Vasc Biol. 2018 Jan;38(1):218-31.

40. Pathak P, Helsley RN, Brown AL, Buffa JA, Choucair I, Nemet I, et al. Small molecule inhibition of gut microbial choline trimethylamine lyase activity alters host cholesterol and bile acid metabolism. Am J Physiol Heart Circ Physiol. 2020;318(6):H1474-86.

41. Turnbaugh PJ, Bäckhed F, Fulton L, Gordon JI. Diet-induced obesity is linked to marked but reversible alterations in the mouse distal gut microbiome. Cell Host Microbe. 2008 Apr 17;3(4):213-23.

42. Turnbaugh PJ, Ridaura VK, Faith JJ, Rey FE, Knight R, Gordon JI. The effect of diet on the human gut microbiome: a metagenomic analysis in humanized gnotobiotic mice. Sci Transl Med. 2009 Nov 11;1(6):6ra14.

43. Lozupone CA, Stombaugh JI, Gordon JI, Jansson JK, Knight R. Diversity, stability and resilience of the human gut microbiota. Nature. 2012 Sep 13;489(7415):220-30.

44. Jarvis KG, Daquigan N, White JR, Morin PM, Howard LM, Manetas JE, et al. Microbiomes Associated With Foods From Plant and Animal Sources. Front Microbiol. 2018 Oct 23;9:2540.

45. Wang HH, Manuzon M, Lehman M, Wan K, Luo H, Wittum TE, et al. Food commensal microbes as a potentially important avenue in transmitting antibiotic resistance genes. FEMS Microbiol Lett. 2006 Jan;254(2):226-31.

46. Bosshard PP, Zbinden R, Altwegg M. Turicibacter sanguinis gen. nov., sp. nov., a novel anaerobic, Gram-positive bacterium. Int J Syst Evol Microbiol. 2002 Jul;52(Pt 4):1263-6.

47. De Filippis F, Pasolli E, Ercolini D. The food-gut axis: lactic acid bacteria and their link to food, the gut microbiome and human health. FEMS Microbiol Rev. 2020 Jun 18;44(4):454-89.

48. Perez-Lopez A, Behnsen J, Nuccio S-P, Raffatellu M. Mucosal immunity to pathogenic intestinal bacteria. Nat Rev Immunol. 2016 Mar;16(3):135-48.

49. Kovaleva J, Degener JE, van der Mei HC. Methylobacterium and Its Role in Health Care-Associated Infection. J Clin Microbiol. 2014 May 1;52(5):1317-21.

50. Osdaghi E, Young AJ, Harveson RM. Bacterial wilt of dry beans caused by Curtobacterium flaccumfaciens pv. flaccumfaciens: A new threat from an old enemy. Mol Plant Pathol. 2020 Feb 25;21(5):605-21.

51. Brown JM, Hazen SL. The Gut Microbial Endocrine Organ: Bacterially-Derived Signals Driving Cardiometabolic Diseases. Annu Rev Med. 2015;66:343-59.

52. Qin J, Li R, Raes J, Arumugam M, Burgdorf KS, Manichanh C, et al. A human gut microbial gene catalog established by metagenomic sequencing. Nature. 2010 Mar 4;464(7285):59-65.

53. Structure, Function and Diversity of the Healthy Human Microbiome. Nature. 2012 Jun 13;486(7402):207-14.

54. McDonald D, Hyde E, Debelius JW, Morton JT, Gonzalez A, Ackermann G, et al. American Gut: an Open Platform for Citizen Science Microbiome Research. mSystems. 2018 Jun;3(3):e00031-18.

55. Everard A, Geurts L, Caesar R, Van Hul M, Matamoros S, Duparc T, et al. Intestinal epithelial MyD88 is a sensor switching host metabolism towards obesity according to nutritional status. Nat Commun. 2014 Dec 5;5:5648.

56. Guo X, Li J, Tang R, Zhang G, Zeng H, Wood RJ, et al. High Fat Diet Alters Gut Microbiota and the Expression of Paneth Cell-Antimicrobial Peptides Preceding Changes of Circulating Inflammatory Cytokines. Mediators Inflamm. 2017;2017:9474896.

57. Liu W, Crott JW, Lyu L, Pfalzer AC, Li J, Choi S-W, et al. Diet- and Genetically-induced Obesity Produces Alterations in the Microbiome, Inflammation and Wnt Pathway in the Intestine of Apc+/1638N Mice: Comparisons and Contrasts. J Cancer. 2016 Aug 12;7(13):1780-90.

58. Hou Y-P, He Q-Q, Ouyang H-M, Peng H-S, Wang Q, Li J, et al. Human Gut Microbiota Associated with Obesity in Chinese Children and Adolescents. Biomed Res Int. 2017;2017:7585989.

59. Zeng Q, Li D, He Y, Li Y, Yang Z, Zhao X, et al. Discrepant gut microbiota markers for the classification of obesity-related metabolic abnormalities. Sci Rep. 2019 Sep 17;9(1):13424.

60. David LA, Maurice CF, Carmody RN, Gootenberg DB, Button JE, Wolfe BE, et al. Diet rapidly and reproducibly alters the human gut microbiome. Nature. 2014 Jan 23;505(7484):559-63.

61. Carmody RN, Bisanz JE, Bowen BP, Maurice CF, Lyalina S, Louie KB, et al. Cooking shapes the structure and function of the gut microbiome. Nat Microbiol. 2019 Dec;4(12):2052-63.

62. Audenaert P, Van Parys T, Brondel F, Pickavet M, Demeester P, Van de Peer Y, et al. CyClus3D: a Cytoscape plugin for clustering network motifs in integrated networks. Bioinformatics. 2011 Jun 1;27(11):1587-8.

63. Zhao M, Zhao L, Xiong X, He Y, Huang W, Liu Z, et al. TMAVA, a Metabolite of Intestinal Microbes, Is Increased in Plasma From Patients With Liver Steatosis, Inhibits γ-Butyrobetaine Hydroxylase, and Exacerbates Fatty Liver in Mice. Gastroenterology. 2020 Jun;158(8):2266-81.e27.

64. Bowerman KL, Rehman SF, Vaughan A, Lachner N, Budden KF, Kim RY, et al. Disease-associated gut microbiome and metabolome changes in patients with chronic obstructive pulmonary disease. Nat Commun. 2020 Nov 18;11(1):5886.

65. Gao B, Duan Y, Lang S, Barupal D, Wu T-C, Valdiviez L, et al. Functional Microbiomics Reveals Alterations of the Gut Microbiome and Host Co-Metabolism in Patients With Alcoholic Hepatitis. Hepatol Commun. 2020 Aug;4(8):1168-82.

66. Kikuchi K, Saigusa D, Kanemitsu Y, Matsumoto Y, Thanai P, Suzuki N, et al. Gut microbiome-derived phenyl sulfate contributes to albuminuria in diabetic kidney disease. Nat Commun. 2019 Apr 23;10(1):1835.

67. Salous AK, Panchatcharam M, Sunkara M, Mueller P, Dong A, Wang Y, et al. Mechanism of rapid elimination of lysophosphatidic acid and related lipids from the circulation of mice. J Lipid Res. 2013 Oct;54(10):2775-84.

68. Kaffe E, Magkrioti C, Aidinis V. Deregulated Lysophosphatidic Acid Metabolism and Signaling in Liver Cancer. Cancers. 2019 Oct 23;11(11)1626.

69. D'Souza K, Paramel GV, Kienesberger PC. Lysophosphatidic Acid Signaling in Obesity and Insulin Resistance. Nutrients. 2018 Mar 23;10(4):399.

70. Madeo F, Eisenberg T, Pietrocola F, Kroemer G. Spermidine in health and disease. Science. 2018 Jan 26;359(6374):eaan2788.

71. Eisenberg T, Abdellatif M, Schroeder S, Primessnig U, Stekovic S, Pendl T, et al. Cardioprotection and lifespan extension by the natural polyamine spermidine. Nat Med. 2016 Dec;22(12):1428-38.

72. Guo Y, Ye Q, Deng P, Cao Y, He D, Zhou Z, et al. Spermine synthase and MYC cooperate to maintain colorectal cancer cell survival by repressing Bim expression. Nat Commun. 2020 Jun 26;11(1):3243.

73. Warrier M, Shih DM, Burrows AC, Ferguson D, Gromovsky AD, Brown AL, et al. The TMAO Generating Enzyme Flavin Monooxygenase 3 is a Central Regulator of Cholesterol Balance. Cell Rep. 2015 Jan 14;10(3):326-38.

74. Miao J, Ling AV, Manthena PV, Gearing ME, Graham MJ, Crooke RM, et al. Flavin-containing monooxygenase 3 as a potential player in diabetes-associated atherosclerosis. Nat Commun. 2015 Apr 7;6:6498.

75. Schugar RC, Shih DM, Warrier M, Helsley RN, Burrows A, Ferguson D, et al. The TMAO-Producing Enzyme Flavin-Containing Monooxygenase 3 Regulates Obesity and the Beiging of White Adipose Tissue. Cell Rep. 2017 Jun;19(12):2451-61.

76. Shih DM, Wang Z, Lee R, Meng Y, Che N, Charugundla S, et al. Flavin containing monooxygenase 3 exerts broad effects on glucose and lipid metabolism and atherosclerosis. J Lipid Res. 2015 Jan;56(1):22-37.

77. Panda S. The arrival of circadian medicine. Nat Rev Endocrinol. 2019 Feb;15(2):67-9.

78. Staels B. When the Clock stops ticking, metabolic syndrome explodes. Nat Med. 2006 Jan;12(1):54-5; discussion 55.

79. Shimizu I, Yoshida Y, Minamino T. A role for circadian clock in metabolic disease. Hypertens Res. 2016 Jul;39(7):483-91.

80. Wang Y, Kuang Z, Yu X, Ruhn KA, Kubo M, Hooper LV. The intestinal microbiota regulates body composition through NFIL3 and the circadian clock. Science. 2017;357(6354):912-6.

81. Kuang Z, Wang Y, Li Y, Ye C, Ruhn KA, Behrendt CL, et al. The intestinal microbiota programs diurnal rhythms in host metabolism through histone deacetylase 3. Science. 2019 Sep 27;365(6460):1428-34.

82. Sato H, Zhang LS, Martinez K, Chang EB, Yang Q, Wang F, et al. Antibiotics Suppress Activation of Intestinal Mucosal Mast Cells and Reduce Dietary Lipid

Absorption in Sprague-Dawley Rats. Gastroenterology. 2016 Nov;151(5):923-32.

83. Hua H, Zhang Y, Zhao F, Chen K, Wu T, Liu Q, et al. Celastrol inhibits intestinal lipid absorption by reprofiling the gut microbiota to attenuate high-fat diet-induced obesity. iScience. 2021 Feb 19;24(2):102077.

84. Hooper LV, Littman DR, Macpherson AJ. Interactions Between the Microbiota and the Immune System. Science. 2012 Jun 8;336(6086):1268-73.

85. Belkaid Y, Hand TW. Role of the Microbiota in Immunity and Inflammation. Cell. 2014 Mar 27;157(1):121-41.

86. Round JL, Mazmanian SK. The gut microbiome shapes intestinal immune responses during health and disease. Nat Rev Immunol. 2009 May;9(5):313-23.